Available online at www.sciencedirect.com
SCIENCE DIRECT
Catalysis Today 116 (2006) 38–49
CATALYSIS TODAY
www.elsevier.com/locate/cattod

H_2 reduction behavior and NO/N_2O abatement catalytic activity of manganese based spinels doped with copper, cobalt and iron ions

Giuseppe Fierro [a,*], Giovanni Ferraris [a], Roberto Dragone [a], Mariano Lo Jacono [b], Marco Faticanti [b]

[a] *Istituto dei Sistemi Complessi del CNR, Gruppo 'Materiali Inorganici e Catalisi Eterogenea', c/o Dipartimento di Chimica, Università 'La Sapienza', P.le A. Moro 5, 00185 Roma, Italy*
[b] *Dipartimento di Chimica, Università 'La Sapienza', P.le A. Moro 5, 00185 Roma, Italy*

Available online 3 May 2006

Abstract

In this work results concerning a study of the effect of Cu, Co, Fe metal ions on the redox properties and on the catalytic behavior of zinc manganite spinels in reactions for the abatement of NO and N_2O are reported. These solids were prepared by thermal decomposition in air at 723 and 973 K of monophasic carbonate precursors. The catalyst reduction in H_2 was investigated by temperature-programmed reduction (TPR). The TPR study makes evident that the spinel reducibility is affected by doping with the transition metal ions which, depending on their nature, play a different role. The reduction is (i) inhibited by iron in some extent, (ii) it was almost unchanged by cobalt and (iii) it is markedly enhanced by copper. The presence of the transition metal ion enhances the catalytic activity of pure zinc manganite for the NO reduction by hydrocarbons and the copper-containing spinel resulted the most active catalyst followed by the iron- and cobalt-doped catalysts. In the case of N_2O reduction by hydrocarbons the catalytic activity resulted much less affected by the doping of the catalysts, in particular when propane is the reductant. All catalysts are stable in the whole range of temperature explored when propane is contained in the reactant stream. By contrast when propene was used as reductant the original catalyst structure was preserved up to about 773 K but, for temperatures equal or higher than this value, the monophasic catalysts fully disgregated by reduction of Mn^{3+} ions to Mn^{2+}ions, and a complex mixture of MnO and ZnO oxides and their reciprocal solid solutions were formed. The only exception is represented by the iron-doped catalyst that, under the propene containing stream, was only partially reduced, this well paralleling the TPR results. In spite of collapsing of the initial monophasic spinel phase, the polyphasic catalysts still maintained a good catalytic activity. This surprising result was explained by suggesting that the Mn^{3+} active species might be regenerated in the reactant stream through the surface oxidation of Mn^{2+} ions by NO, or N_2O.

Keywords: Copper-zinc manganites; Cobalt-zinc manganites; Iron-zinc manganites; Carbonate precursors; Temperature-programmed reduction; NO and N_2O reduction by propane and propene; NO and N_2O decomposition

1. Introduction

The NO and N_2O nitrogen oxides are well known to have detrimental effects on the environment like ground-level ozone formation, greenhouse effect and acid deposition. The removal of these pollutants from exhaust gases, produced by both stationary and mobile sources, and the reduction of their emission in the atmosphere are nowadays world-wide demanding tasks and research about this matter is considerably on the increase [1,2]. Different catalytic systems have been investigated to convert NO and N_2O into N_2 either by direct decomposition or by reaction with a reductant and recently manganese-based catalysts have received a renewed attention for such reactions [3–9]. Some years ago we started a research project concerning the preparation and characterization of transition metal ions containing zinc manganite spinels because they seemed to be catalysts of interest for reactions in which NO and N_2O are turned into N_2 [9]. Spinels, having the possibility of replacing cations in both the tetrahedral and octahedral sites available in the crystal lattice, are suitable for fundamental studies to find a correlation between structural and redox, or catalytic, properties of the catalyst. In this work a comparison of the effect of copper, cobalt and iron hosted ions on the reduction in H_2 of the $ZnMn_2O_4$ spinel as well as on its

* Corresponding author. Fax: +39 06 490324.
E-mail address: giuseppe.fierro@uniroma1.it (G. Fierro).

0920-5861/$ – see front matter © 2006 Elsevier B.V. All rights reserved.
doi:10.1016/j.cattod.2006.03.006

catalytic activity is reported. The reduction behavior in H_2 was studied by temperature-programmed reduction (TPR) whereas the catalytic activity was tested for the abatement of NO and N_2O, via reduction by hydrocarbons or direct decomposition, in the range of temperature 523–873 K. For the NO and N_2O reduction, propane and propene were used as reductants.

2. Experimental

2.1. Catalyst preparation

Carbonate precursors were obtained by coprecipitation at constant pH starting from an aqueous solution of metal salts. In order to obtain after thermal decomposition spinel-like structures, i.e. $Me^{2+}[Me^{3+}]_2O_4$, the Mn/(Zn + Me) ratio (Me = Cu, or Co, or Fe) was fixed at 2 while the Me/(Zn + Me) ratio (x) was changed from 0.01 to 0.10. With this respect, in order to make a better comparison, since the solids showed similar characteristics regardless the transition metal ion loading, the precursors and catalysts with the highest transition metal content ($x = 0.10$) were chosen as representative to compare to each other and to the $x = 0$ preparation. Suitable amounts of $Mn(NO_3)_2$ and $Zn(NO_3)_2{\cdot}6H_2O$ (Carlo Erba RPE reagent grades) were mixed to $Cu(NO_3)_2{\cdot}3H_2O$ (Carlo Erba RPE reagent grade), or $Co(NO_3)_2{\cdot}6H_2O$ (Carlo Erba RPE reagent grade), or $FeCl_2{\cdot}4H_2O$ (Fluka reagent) in 0.5 L of distilled water. This solution was then rapidly added to 1 L of a $NaHCO_3$ vigorously stirred and held at the temperature of about 313 K. The slurry was aged for 1.5 h. The precipitate was first washed by filtration with distilled water and then dried in an oven for about 20 h at 363 K. The final catalysts were obtained by decomposition of the precursors in air at 723 and 973 K for 24 h. The catalysts prepared at both temperatures have been labelled as ZnMn-Me(x), where x = Me/(Me + Zn) = 0 or 0.10 with reference to the transition metal ion content in the catalyst.

2.2. Precursor and catalyst characterization

Both precursors and catalysts have been characterized by different techniques. Experimental details about the structural characterization of both precursors and catalysts can be found elsewhere [9–11]. Briefly, Mn, Zn, Cu, Co, Fe elemental analyses were performed by atomic absorption (Varian SpectrAA-30 instrument), the X-ray diffraction (XRD) patterns of powders were obtained with a Philips automated PW 1729 diffractometer equipped with a computer for data acquisition and analysis (software APD-Philips). Scans were taken with a 2θ step size of 0.01° and using Cu Kα (nickel-filtered) radiation. XRD reference spectra for hydroxycarbonates and oxides were taken from literature.[1] The specific surface area (S.S.A.) of the catalysts after calcination at 723 and 973 K were measured by the BET method using a Micromeritics ASAP 2010 apparatus and nitrogen ($\sigma_{N_2} = 0.162$ nm^2) or krypton ($\sigma_{Kr} = 0.195$ nm^2) as adsorbates. The magnetic susceptibility per gram of sample, χ_{sp}, was measured by the Gouy method in the temperature range of 100–300 K [9]. A Mössbauer analysis for the identification of the iron chemical state and its coordination symmetry was made. Details of this study have been reported elsewhere [11].

2.3. Temperature-programmed reduction

Temperature-programmed reduction (TPR) experiments were carried out with a home-made apparatus [12]. It consists of the following parts: (i) an in-flow system equipped with a 4-channel electronic mass-flow controller (Brooks Instrument, Model 5850S) to fix the flow of the He, N_2, H_2 and O_2 ultra pure gases, (ii) a BET-type vacuum line where the sample pretreatment, trapping of the water released during the reduction and measurement of its quantity can be effected [12], (iii) a hot wire (HW) detector from Carlo Erba (Model HWD 450), (iv) a temperature controller (Leeds & Northrup Instrument, Model Electromax V Plus) for the temperature programs, (v) a personal computer, for data acquisition and processing, at which both the HW detector and the temperature controller were connected. The reduction profiles have been optimized avoiding the interference by artifacts. To this purpose the experimental operating variables, i.e. the initial hydrogen concentration ($c_o = 2.52$ μmol mL^{-1}), the initial amount of reducible species ($S_o = 100$–180 μmol), the total flow rate ($V_{tot} = 40$ mL min^{-1}) were carefully chosen and combined in order to obtain correct values of the 'K' parameter ($55\ \text{s} < K = S_o\ (V_{tot}c_o)^{-1} < 140\ \text{s}$, at the heating rate of $\beta = 5$ K min^{-1}) [12–14]. Before starting a TPR run, each sample was pretreated in situ overnight under flowing O_2 (10%, v/v, in He) at 673, or 773 K, depending on the calcination temperature (723 and 973 K, respectively), followed by cooling in the same stream to 623 K and flushing with He at this temperature for 0.25 h. The sample was then cooled in N_2 to room temperature and maintained in this condition for 0.5 h. Next, by mixing in suitable proportion the N_2 and H_2 flows, the reducing blend (40 mL min^{-1} of 6%, v/v, H_2 in N_2) was passed through the reactor and then, at its outlet, through the vacuum line trap cooled with liquid nitrogen in which oxygen was in advance bubbled for a few minutes. A standard TPR run consisted of (a) an initial treatment in the reducing gas flow at room temperature for 0.01 h, (b) temperature programming, and (c) outgassing of the sample at the final temperature for 0.5 h. The heating rate was fixed at 5 K min^{-1}. The total hydrogen consumption was determined in two ways: (i) by integration of the HW detector signal with an integrator (Shimadzu Instruments, Model Chromatopac C-R6A); (ii) by estimating the water released and trapped during the reduction through a stepwise expansion into a calibrated zone of the vacuum line. Peaks in the TPR profiles were characterized by the temperature at the maximum hydrogen consumption rate, T_M, and the full width at half maximum, $W_{1/2}$. The reproducibility of both the peak shape and the peak maximum has been checked and we found that it was always preserved. Under the experimental conditions used in this work, the confidence limits for the H_2 quantitative analysis and for the

[1] X-ray powder data file: (a) ASTM 7–268 for $MnCO_3$ (rhodochrosite); (b) ASTM 24–1133 for $ZnMn_2O_4$ (hetaerolite); (c) ASTM 36-1451 for ZnO (zincite); (d) ASTM 7-230 for MnO (manganosite).

temperature corresponding to the peak maximum (T_M) are ±5% and ±10 K, respectively.

2.4. Catalytic tests

The catalytic tests were carried out in the steady state flow mode. The apparatus consists of a flow system, with valves and capillary tubing of stainless steel to perform the reaction studies, connected to a Pyrex made vacuum line where the catalyst pretreatment was made in situ [15]. The reactant gases were of high purity grade (99.999%) and were used as received. Ultrapure grade helium was used as diluent. The flow of each gas was fixed and held constant with a 4-channel electronic mass-flow controller (Brooks Instrument, Model 5850S). The effluent gas was sampled and analyzed by an on-line gas chromatograph (DANI Instruments, Model 3800) provided with an Alltech CTR-1 column and a hot wire detector from DANI (Model HWD 686). The quantitative analysis was made by transmitting the HW detector output to an amplification and integration system (Shimadzu Instruments, Model Chromatopac C-R6A). A temperature controller (Leeds & Northrup Instruments, Model Electromax V Plus) was used both for increasing the furnace temperature by linear heating rates (10 K min^{-1}) and for keeping it constant at any selected value. Since the maximum reaction temperature explored was 873 K, the catalysts calcined at 973 K were selected for the catalytic runs. Depending on the catalytic activity, the catalyst loading was changed from ca. 50 mg up to 250 mg so that the conversions were low enough for calculating reliable apparent reaction rates. The catalysts were loaded in a quartz-glass reactor and, before reaction, they underwent the following standard pretreatment: (i) flowing O_2 at 923 K overnight, (ii) cooling in O_2 at 573 K, (iii) flushing with dried He for about 15 min. at this temperature and, finally, (iv) cooling at room temperature before the reaction was initiated. The typical reactant blend, 0.46% NO (or 0.46% N_2O) + 0.46% C_3H_8 (or C_3H_6) + He to balance, for the reduction reaction, or 0.46% NO (or 0.46% N_2O) + He to balance, for the decomposition reaction, was passed over the catalyst while the temperature was linearly increased, or decreased, in the range 523-873 K with a 0.5 h isothermal steps at any selected temperature value during which the analysis of the effluent gas was made. In any experiment the total flow rate was kept constant at 100 mL(NTP) min^{-1} and pure He was used to maintain the total pressure at 1 atm. Under these conditions GHSV ranged from 12,000 to 60,000 h^{-1}. Nitrogen and carbon balances were always better than 95%. Blank experiments carried out by flowing the reactant streams over an empty reactor showed that no conversion occurred up to 873 K.

3. Results and discussion

3.1. Precursors and catalysts characterization

In Table 1 some results of the characterization of the precursors and the final catalysts are summarized. The XRD patterns of all the precursors are very similar regardless the presence of the transition metal ion, its nature (Cu, Co or Fe) and content. In Fig. 1A the XRD spectra of the $x = 0$ and $x = 0.10$ compositions are reported and they are compared with the reference lines of rhodochrosite ($MnCO_3$) (see footnote 1(a)). As shown by Fig. 1A, the diffraction patterns of the precursors matched that of the rhodochrosite reference compound and, within the sensitivity limits of the technique, no extra phases were detected. This suggests that the precursors are monophasic and made by a solid solution of zinc alone or zinc plus iron, or cobalt, or copper ions into the $MnCO_3$ rhombohedral lattice. A careful inspection of the position of the XRD lines evidenced a systematic shift of the diffraction peaks towards higher 2θ values (lower d spacing) on comparing with the $MnCO_3$ reference spectrum. We made this evident in Fig. 1B reporting a magnification of a portion of the XRD spectra of Fig. 1A. An explanation can be given if the cation relative sizes are taken into account. Since Zn^{2+}(0.74 Å), Fe^{3+} (0.645 Å), Fe^{2+} (0.75 Å), Co^{2+} (0.745 Å), and Cu^{2+} (0.73 Å) have a smaller ionic radius than Mn^{2+} (0.83 Å) in octahedral coordination [16], their presence in a rhodochrosite-like solid solution, i.e. $Zn_{0.33}Mn_{0.67}CO_3$ or $Me_{0.03}Zn_{0.30}Mn_{0.67}CO_3$ (Me = Fe, or Co, or Cu), can result in an overall shrinkage of the unitary cell with respect to the pure compound. The Mössbauer study of the iron containing precursors showed a massive presence of Fe^{3+} ions (see Table 1 and [11]). If, on one hand, it is possible that Fe^{2+} as well as Zn^{2+} ions can enter the rhodochrosite structure forming solid solution with Mn^{2+} even

Table 1
Precursors and catalysts characterization

Sample x = Me/(Me + Zn) (Me = Cu, Co, Fe)	$T_{cal.}$ (K)	XRD phase	Surface area (m^2 g^{-1})			Transition metal ion chemical state and symmetry				
			Cu	Co	Fe	Mn	Cu	Co	Fe	
Precursor										
$Zn_{0.33}Mn_{0.67}CO_3$ ($x = 0$)	383	R[a]				Mn^{2+}/Oh	–	–	–	–
$Me_{0.03}Zn_{0.30}Mn_{0.67}CO_3$ ($x = 0.10$)	383	R				Mn^{2+}/Oh	Cu^{2+}/Oh	Co^{2+}/Oh	Fe^{2+}/Oh (5%)	Fe^{3+}/Oh (95%)
Calcined catalysts										
$ZnMn_2O_4$	723	S[b]	49	49	49	Mn^{3+}/Oh	–	–	–	–
ZnMn-Me(0.10)	723	S	36	44	41	Mn^{3+}/Oh	Cu^{2+}/Td	Co^{3+}/Oh	–	Fe^{3+}/Oh
$ZnMn_2O_4$	973	S	6.2	6.2	6.2	Mn^{3+}/Oh	–	–	–	–
ZnMn-Me(0.10)	973	S	2.9	6.2	6.1	Mn^{3+}/Oh	Cu^{2+}/Td	Co^{3+}/Oh	–	Fe^{3+}/Oh

[a] R: Rhodochrosite-like ($MnCO_3$).
[b] S: Tetragonal spinel-like ($ZnMn_2O_4$).

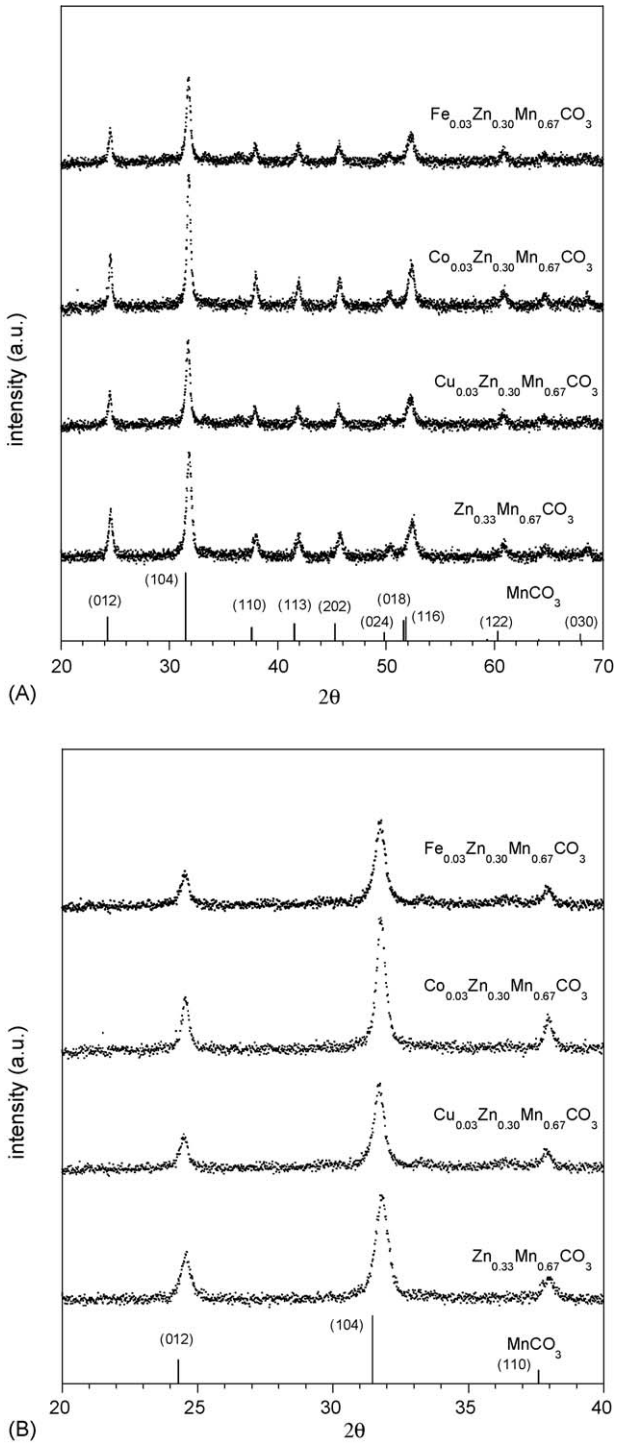

Fig. 1. (A) XRD patterns (Cu Kα radiation) of the $Me_{0.03}Zn_{0.30}Mn_{0.67}CO_3$ carbonate precursors (Me = Cu, Co, Fe)). For the sake of comparison the reference spectrum of $MnCO_3$ (rhodochrosite, see footnote 1(a)) and its indexing are also included. (B) Magnification of a portion of the XRD spectra reported in (A) for making evident the systematic shift of diffraction peaks.

to a large extent, being the charge and size criteria both satisfied, how, on the other hand, can the Fe^{3+} ions be hosted in the $Zn_xMn_{1-x}CO_3$ crystal structure? For each Fe^{3+} ion coming in, a positive charge in excess is brought into the lattice. In order to preserve the crystal electrical neutrality, such a charge increase must be compensated. This can be done through creation of Zn^{2+} or Mn^{2+} vacancies according to the following reaction:

$$3Me^{2+} \rightarrow 2Me^{3+} + \square_v \quad (1)$$

Accordingly, the following type-formula may be proposed for the iron containing carbonate precursors:

$$Mn_{(1-x-y)}{}^{2+}Zn_x{}^{2+}Fe_{(y-\alpha)}{}^{2+}Fe_{(2/3)\alpha}{}^{3+}\square_{\alpha/3}CO_3 \quad (2)$$

However, we cannot exclude that a surface hydration of the precursors may induce the oxidation of Fe^{2+} ions through formation of Fe^{3+}-OH hydroxylated species. In any case it is relevant that, besides Zn^{2+}, $MnCO_3$ is able to accommodate Fe^{3+} ions in its lattice, at least at the small Fe atom loading of our samples (ca. 3 wt.%). The XRD patterns of the catalysts calcined at 723 and 973 K are reported, respectively, in Fig. 2A and B together with the reference pattern of hetaerolite, $ZnMn_2O_4$ (see footnote 1(b)). At both calcination temperatures the XRD patterns of all calcined samples matched very closely that of the hetaerolite reference compound and no lines of other phases appeared in their spectra. The catalysts calcined at 973 K were characterized by a higher crystallinity when compared to those of the homologous samples decomposed at 723 K. This is reflected by the values of the specific surface areas that drastically decreased for the catalysts calcined at 973 K, clearly indicating that much larger particles are formed at this temperature (see Table 1). The sample ZnMn-Me(0) (having no transition metal ions) crystallizes as hetaerolite, i.e. $Zn^{2+}[Mn^{3+}]_2O_4$, in a distorted spinel structure where the O^{2-} anions form a close-packed tetragonal lattice in which the Zn^{2+} and Mn^{3+} cations are located in tetrahedral sites (labelled as A sites) and octahedral sites (labelled as B sites), respectively, giving a configuration called 'normal' spinel [17,18]. The samples ZnMn-Fe(0.10), ZnMn-Co(0.10) and ZnMn-Cu(0.10) still crystallize as hetaerolite (see Fig. 2) thus indicating that iron, cobalt and copper ions enter in solid solution in the $ZnMn_2O_4$ spinel lattice. According to magnetic and Mössbauer analyses [9–11], upon thermal decomposition of the precursors Cu^{2+} ions do not change, as expected, their chemical state but iron and cobalt do: in the Fe-catalysts the residual amount of Fe^{2+} found in the precursors turns into Fe^{3+}, and the Co^{2+} ions turns totally into Co^{3+} ions in the cobalt containing catalysts (see Table 1). The Cu^{2+} ions are located in the tetrahedral sites of the spinel structure together with the Zn^{2+} ions [9] giving rise to the $Zn_{1-x}Cu_xMn_2O_4$ compounds. On the other hand, Co^{3+} ions [10] or Fe^{3+} ions as well [11] partially replace the Mn^{3+} ions in the spinel octahedral sites. In order to preserve the crystal electrical neutrality, the Mn^{3+} ions pushed out from the octahedral sites should turn into Mn^{2+} ions that are likely to migrate in the tetrahedral sites. Accordingly, the final picture of the copper-, cobalt- and iron-containing catalysts may be represented by the following formulas:

$$Zn_{1-x}{}^{2+}Cu_x{}^{2+}[Mn^{3+}]_2O_4 \quad (3)$$

$$Zn_{1-x}{}^{2+}Mn_x{}^{2+}[Mn_{2-x}{}^{3+}Co_x{}^{3+}]O_4 \quad (4)$$

$$Zn_{1-x}{}^{2+}Mn_x{}^{2+}[Mn_{2-x}{}^{3+}Fe_x{}^{3+}]O_4 \quad (5)$$

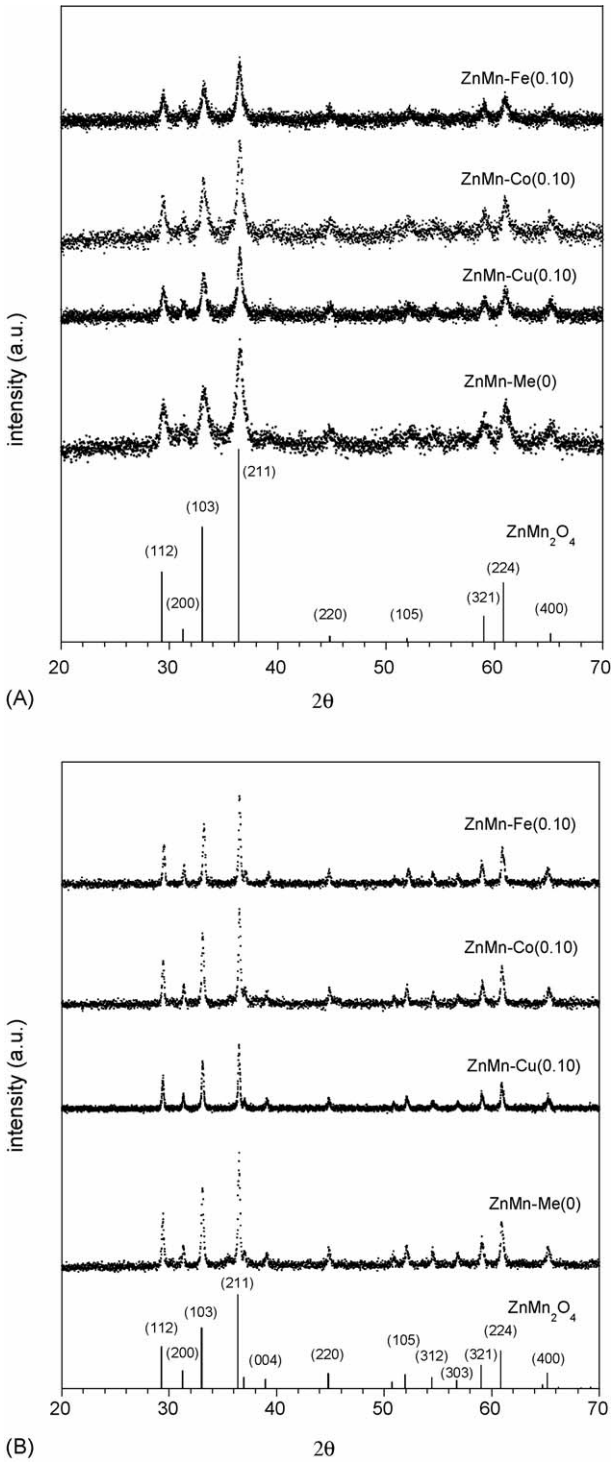

Fig. 2. XRD patterns (Cu Kα radiation) of the ZnMn-Me(0) and ZnMn-Me(0.10) catalysts calcined (A) at 723 K and (B) at 973 K (Me = Cu, Co, Fe). For the sake of comparison the reference spectrum of $ZnMn_2O_4$ (hetaerolite, see footnote 1(b)) and its indexing are also included.

3.2. Temperature-programmed reduction

The TPR profiles of the catalysts calcined at 723 and 973 K are reported in Fig. 3A and B, respectively. The results obtained from TPR analysis are summarized in Table 2. In all cases and for both preparations, the hydrogen uptake and the amount of

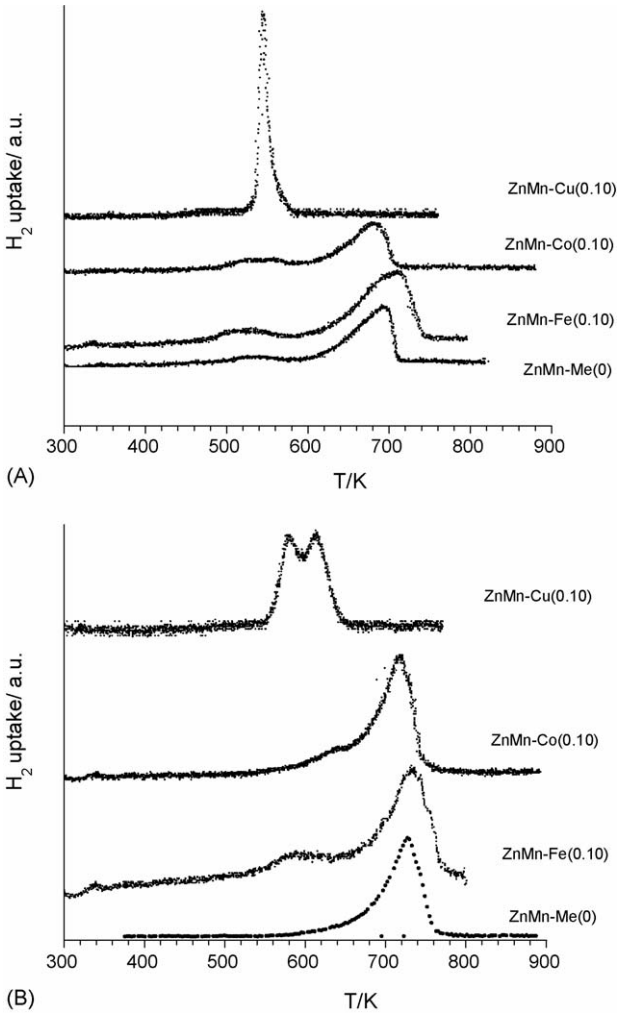

Fig. 3. TPR profiles of $ZnMn_2O_4$ undoped and doped with Cu, Co and Fe ions: (A) catalysts calcined at 723 K, (B) catalysts calcined at 973 K.

water formed upon reduction are consistent with the complete reduction of the $ZnMn_2O_4$ spinel, and its Cu, Co or Fe solid solutions, to MnO and ZnO. This result is supported by the XRD analysis of each catalyst at the end of the TPR run showing only the diffraction lines of ZnO and MnO. In Fig. 4A the XRD patterns next TPR of the catalysts calcined at 973 K are representatively shown together with the reference spectra of ZnO (zincite) and MnO (manganosite) (see footnote 1(c) and (d), respectively). With regard to the solids calcined at 723 K, the reduction profile of $ZnMn_2O_4$ is characterized by a prominent peak centred at 688 K and by a shoulder at lower temperature. The most intense TPR peak can be related to the reduction of Mn^{3+} ions to Mn^{2+} followed by the disgregation of the original spinel phase. The shoulder at the lower temperature side may be related to a different kinetic of the reduction process, i.e. surface oxygen involving reduction, or may arise from the reduction of a very small amount of a manganese oxide homogeneously distributed and finely dispersed over the $ZnMn_2O_4$ particles and not detected by XRD. On the other hand, the TPR profiles of the Cu-, Co-, Fe-doped $ZnMn_2O_4$ catalysts make in evidence that the reduction behavior of the zinc manganite is affected by the presence of the transition

Table 2
TPR results of zinc manganites calcined at 723 and 973 K

Sample ZnMn-Me (Me = Fe, Co, Cu)	T_{calc} (K)	TPR run	T_M (K)[a]	$K = S_o/(Vc_o)$ (s)	$W_{1/2}$ (K)[b]	Loading (g)	S_o (μmol)[c]	$(H_2)_c$ (μmol)[d]	$(H_2O)_r$ (μmol)[e]
ZnMn-Me(0)	723	267A	688 (516)	63	45	0.02548	106	133	125
ZnMn-Fe(0.10)	723	288A	703 (533)	99	70	0.04346	174	193	195
ZnMn-Co(0.10)	723	259A	683 (543)	76	58	0.02648	128	132	118
ZnMn-Cu(0.10)	723	175A	553	60	13	0.02431	102	110	113
ZnMn-Me(0)	973	279A	728	103	48	0.04172	174	187	190
ZnMn-Fe(0.10)	973	290A	733 (593)	93	61	0.04077	163	195	198
ZnMn-Co(0.10)	973	280A	718	109	49	0.03813	184	178	174
ZnMn-Cu(0.10)	973	190A	613 (580)	62	31 (31)	0.02498	104	104	120

Experimental conditions: (a) $\beta = 5$ K min^{-1}, (b) reducing blend: H_2/N_2 (6:94, v/v), (c) total flow rate (V_{tot}) = 40 NmL min^{-1}.
[a] Temperature of peak maximum. In brackets the T_M value of a second peak, or shoulder, on the lower temperature side is reported.
[b] Full width at half maximum of the reduction peak.
[c] Initial amount of the reducible species calculated as the amount of H_2 needed to reduce Mn^{+3} to Mn^{+2} in the spinel.
[d] Hydrogen uptake.
[e] Water released during the reduction and measured 'in situ' at the end of the TPR run (see text).

metal ions which, depending on their nature, play a different role. The TPR profile of the ZnMn-Cu(0.10) sample is still characterized by a single peak but, compared to the $ZnMn_2O_4$, i.e. ZnMn-Me(0) preparation, it is much sharper and remarkably shifted at lower temperature (553 K, see Table 2). Both the shift of the peak maximum (T_M) to lower temperature and the peak sharpening (faster reaction) clearly indicate that the presence of copper in the spinel promotes its reducibility. We found a similar promoting effect of copper for the reduction of Co_xO_y-CuO mixed oxides [19] and Cu-Zn-Cd chromites [20]. Under the same experimental conditions of this work, the TPR of CuO showed a single peak related to the reduction of CuO to Cu^0 with a maximum at 504 K [12,21,22], a temperature considerably lower than that of the $ZnMn_2O_4$ peak maximum (688 K). This suggests that copper (II) oxide is more easily reduced than manganese (III) in $ZnMn_2O_4$. Although in copper-zinc manganite the Cu^{2+} ions located in the tetrahedral sites of the spinel can be partly stabilized towards reduction by the spinel structure, on the basis of their different reducibility with respect to Mn^{3+} ions, they are very likely to be initially reduced to copper metal which enhances the reduction of Mn^{3+} ions, in the octahedral sites, to Mn^{2+}. Consequently, the collapsing of the zinc manganite doped with copper occurs at a remarkably lower temperature with respect to the undoped $ZnMn_2O_4$. TPR profile of the cobalt containing catalyst, ZnMn-Co(0.10), looks like that of $ZnMn_2O_4$ being characterized by a similar peak shape and peak position (see Table 2). This suggests that cobalt, differently from copper, does not have an influence on the spinel reducibility. As revealed by magnetic analysis, upon reduction cobalt metal is formed besides ZnO and MnO thus the final state for reduced cobalt or copper manganites catalysts is very similar, namely ZnO, MnO and a metal phase, copper or cobalt. However, in spite of this similarity, the reduction behavior is quite different. Then, how can the different effect of copper and cobalt be explained? The higher reducibility of copper-zinc manganite with respect to the homologous cobalt-doped sample may be related to the different reducibility of the Cu^{2+} and Co^{3+} cations to metal. The Co^{3+} can be initially reduced to Co^{2+} ions but these latter are much less reducible than Cu^{2+} ions and request a higher energy to be reduced to metal [19], in agreement with the standard redox potentials (E^0 $Co^{2+}/Co^0 = -0.277$V, E^0 $Cu^{2+}/Cu^0 = +0.337$ V). Therefore, according to the different Cu^{2+} and Co^{3+}, or Co^{2+}, reducibility, a realistic picture of the reduction process in the cobalt-zinc manganites is drawn: the reduction of Co^{3+} ions to cobalt metal, as a direct process or by an intermediate reduction to Co^{2+} ions, takes place almost simultaneously to the reduction of the Mn^{3+} ions to Mn^{2+} ions in a such a way that the TPR peak does not differ from that of the pure $ZnMn_2O_4$. With regard to iron-doped zinc manganite, its TPR profile is similar in shape to those observed for either the undoped $ZnMn_2O_4$ and the homologous cobalt-doped samples (see Fig. 2) but, if compared to both of them, the maximum of the reduction peak is shifted towards higher temperature (see Table 2). This suggests that the spinel becomes more resistant toward reduction when Fe^{3+} ions are present in its structure. The chemistry of iron ions is helpful for understanding the difference in reactivity with respect to the copper and cobalt systems. Similarly to Co^{3+} ions, also the Fe^{3+} ions may be reduced first to Fe^{2+} but the further reduction of Fe^{2+} to Fe^0 will be very difficult as expected on the basis of the standard reduction potential (E^0 $Fe^{2+}/Fe^0 = -0.44$V, E^0 $Co^{2+}/Co^0 = -0.277$ V). This is supported by the fact that, in spite of many efforts, no evidence of iron metal was found in the reduced iron-zinc manganite sample. These iron characteristics are likely to make the spinel more resistant towards reduction. With the only exception of the ZnMn-Cu(0.10) sample, the TPR profiles of the catalysts calcined at 973 K are similar to those of the homologous preparations at 723 K being present a single reduction peak whose maximum, however, is shifted towards higher temperature (see Fig. 3B). The shoulder appearing at lower temperature in some reduction profiles of the samples calcined at 723 K disappeared as the calcination temperature was increased, pointing out that it was probably related to some surface species, or process, which vanished by catalyst sintering. As for the catalysts calcined at 723 K, the hydrogen uptake was almost equivalent to the amount expected to be consumed by the loaded portion of catalyst on the basis of the total reduction to MnO and ZnO, and the H_2O formed by reduction paralleled the H_2 consumption. The increase of the

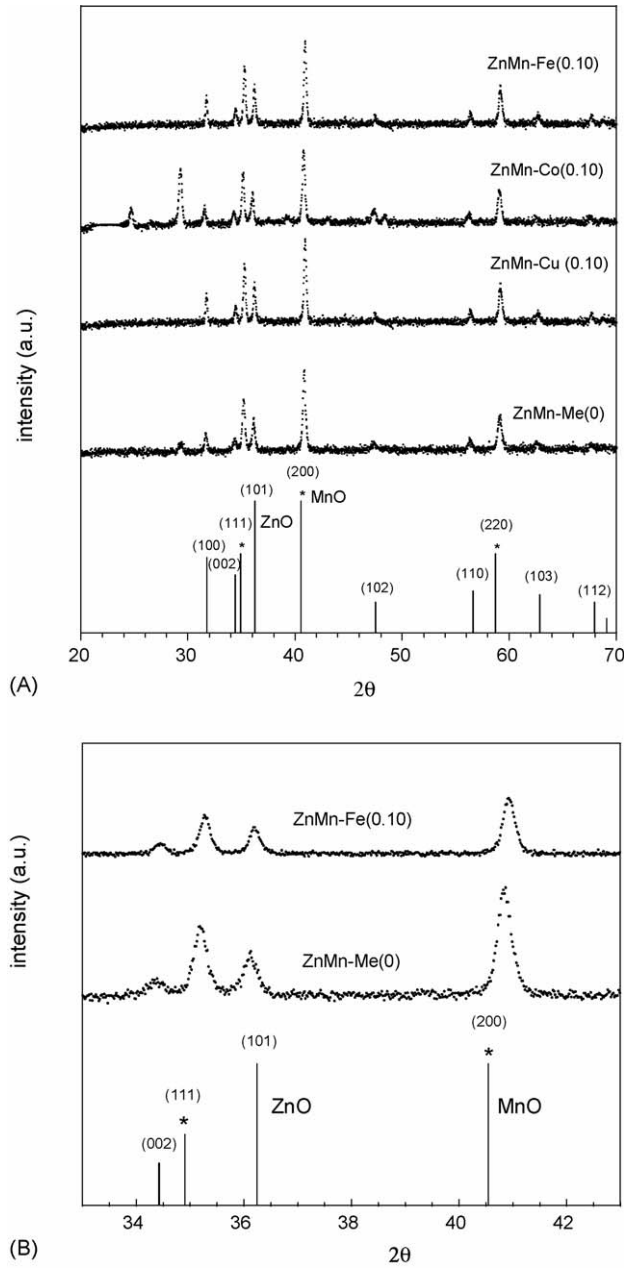

Fig. 4. (A) XRD patterns (Cu Kα radiation) recorded after TPR of the catalysts calcined at 973 K. For the sake of comparison, the reference spectra of ZnO (zincite, see footnote 1(c)) and of MnO (manganosite, see footnote 1(d)) together with their indexing are included. (B) Magnification of a portion of the XRD spectra reported in (A) for the $ZnMn_2O_4$, i.e. ZnMn-Me(0), and ZnMn-Fe(0.10) samples for making evident the systematic shift of the ZnO and MnO diffraction peaks. Reference spectra of ZnO (unmarked lines) and MnO (lines marked with asterisks) are also reported.

T_M values for the catalysts calcined at 973 K with respect to those calcined at 723 K is a strong evidence that they are less reducible than the homologous samples calcined at lower temperature. As a consequence, the difference between the T_M values between the ZnMn-Me(0) and the ZnMn-Me(0.10) samples becomes smaller and the effect of the transition metal ion on the spinel reducibility, even if preserved, appear to be smoothed. The difference in reactivity between the samples calcined at 973 and 723 K can be ascribed to the larger particle size obtained on increasing the calcination temperature, as reflected by the values of surface area that dramatically decrease for the preparations at 973 K (see Table 1). The peak splitting in the TPR profile of the ZnMn-Cu(0.10) sample is probably due to kinetic effects induced by two different activation energies for the same main $Mn^{3+} \rightarrow Mn^{2+}$ reduction process. As already anticipated, the XRD analysis of the all reduced catalysts shows the formation of MnO and ZnO oxides. However, by a careful inspection of the reflection positions in the XRD patterns, a systematic shift of the MnO and ZnO diffraction peaks in opposite and, therefore, complementary direction was evidenced. As apparent in Fig. 4B, which shows a magnification of a relevant part of two representative XRD spectra reported in Fig. 4A, the diffraction peaks of MnO were displaced towards higher 2θ angles (lower d spacing) with respect to pure MnO whereas the ZnO peaks were shifted towards lower 2θ angles (higher d spacing) with respect to pure ZnO. These results suggest that solid solution of Zn^{+2} ions in MnO and of Mn^{+2} ions in ZnO are formed upon collapsing of the spinel structure as the reduction proceeded. The observed XRD peaks displacement were also consistent with the expected change of the ZnO and MnO unit cells size upon formation of solid solutions with Mn^{+2} and Zn^{+2} ions according to their ionic radii (0.83 and 0.74 Å in octahedral coordination, respectively) [16].

3.3. Catalytic tests

3.3.1. Reduction of NO by propane or propene

In Fig. 5A and B the Arrhenius plots for the specific surface rate of NO reduction by C_3H_8 (A) and C_3H_6 (B) are reported. With both hydrocarbons, at the highest reaction temperature explored (873 K) the selectivities to N_2 and CO_2 are equal to 100% for any catalyst used. From these plots, ZnMn-Me(0), i.e. $Zn^{2+}[Mn^{3+}]_2O_4$, resulted to be an active catalyst per se clearly indicating that Mn^{3+} ions in octahedral sites of the spinel are active sites in the previous reactions. This is well consistent with literature showing that Mn(III) is the chemical state of manganese always strongly involved in NO adsorption [23] or reactions as decomposition [5] and selective catalytic reduction (SCR) by ammonia [3,6]. Besides, the Arrhenius plots clearly show that the catalytic activity is strongly affected by the presence of the transition metal ion. Indeed, by adding cobalt, iron or copper in the $ZnMn_2O_4$ spinel the catalytic activity increases, the increase depending on the nature of the transition metal ion. These results, as a whole, indicate that the transition metal ions play an active role for the reaction with both hydrocarbons and their action overlap to that of Mn^{3+} ions. Zinc manganite doped with copper is the most active catalyst followed by the iron and cobalt zinc manganites. Accordingly, the following scale of decreasing activity can be drawn:

$$\text{ZnMn-(Cu)} > \text{ZnMn-(Fe)} > \text{ZnMn-(Co)} > \text{ZnMn-Me(0)}\ (ZnMn_2O_4) \quad (6)$$

On switching from propane to propene the trend depicted by the previous scale does not change. However, the Arrhenius

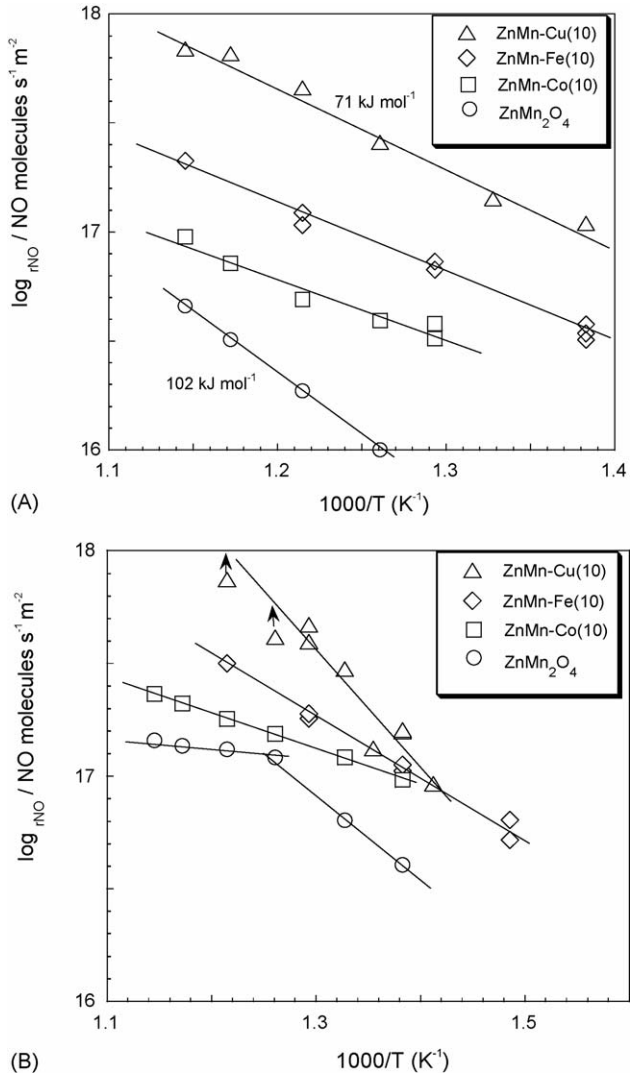

Fig. 5. Arrhenius plot of the NO reduction rates by C_3H_8 (A) and C_3H_6 (B) over the ZnMn-Me(0.10) catalysts. Reactant stream for the reduction [NO] = [C_3H_8] = [C_3H_6] = 4600 ppm + He balance (GHSV = 60,000 h^{-1}).

plots make also in evidence a peculiar catalytic behavior for each hydrocarbon. In the case of NO reduction by propane the activity levels are more splitted from each other, evidencing a greater separation effect. Moreover, the slope of the activity levels of the transition metal ion doped catalysts is very close to each other and significantly lower than that of the activity line of undoped zinc manganite, ZnMn-Me(0) ($ZnMn_2O_4$). This corresponds to a change of the apparent activation energy that increases from ca. 70 kJ mol^{-1} for the ZnMn-(Cu), ZnMn-(Fe) and ZnMn-(Co) catalysts up to ca. 100 kJ mol^{-1} for $ZnMn_2O_4$. The large decrease of the apparent activation energy caused by Cu^{2+}, Fe^{3+} and Co^{3+} ions suggests that they are directly involved in the rate determining step and make the reaction easier to proceed. On the other hand, in the case of propene the activity levels resulted closer suggesting that C_3H_6 is more reactive than propane. The activity lines of the transition metal ion doped catalysts have different slopes and the apparent activation energy increases from cobalt to iron and to copper that, however, still remains the most active catalyst at the highest reaction temperatures. Although we do not have a direct experimental evidence, we suggest that a role of copper could be that to enhance the hydrocarbons adsorption and, consequently, the NO reduction reaction. To a less extent, the role of iron and cobalt should be the same. On the other hand, propane may be rather weakly absorbed but propene can be more strongly bound at the catalyst surface owing to the presence of the π-bonding electrons that, as it is well known on a general ground, give usually to alkenes a much higher adsorption strength than alkanes. Therefore, it is expected that the effect of the transition metal ion doping on the catalytic activity is better observed when the hydrocarbon adsorption is rather weak, as propane, whereas the more strongly adsorbed propene should react more promptly with NO thus partially hiding the transition metal ion effect on the catalytic activity. An indirect proof of the different absorption behavior between propane and propene is given by the selectivity data: if the selectivity to CO_2 is always equal to unity with either propane and propene in the whole range of temperature explored, on the other hand the selectivity to N_2 in the temperature range 693–763 K is lower than unity when the alkene was used as reductant, N_2O being a further reaction product. At first sight this result might appear surprising because an oxidized intermediate like N_2O is formed during the NO reduction by propene which is a stronger reductant than propane. However it can be explained if a competitive adsorption between the reaction intermediate N_2O and propene occurs on the same site according to the following equilibrium:

$$N_2O_{(ads)} + C_3H_{6(g)} \leftrightarrows C_3H_{6(ads)} + N_2O_{(g)} \quad (7)$$

It follows that the desorption rate of the alkene is lower, in particular as the temperature decreases, and consequently the N_2O adsorption on the same site results more difficult according to the equilibrium represented by Eq. (7). This can explain why the N_2 selectivity decreases as N_2O is formed in the gas phase at temperatures lower than 773 K when propene is used as reductant of NO. On the other hand, the Mn^{3+} ions in the octahedral sites of the spinel may act as acid Lewis sites on which NO can adsorb by forming nitrosylic species [6]. Nevertheless, our results parallel recent literature data which indeed showed that manganese, present as isolated Mn^{3+} ions in octahedral coordination, resulted in a very high selectivity towards N_2 production for the SCR of NO by NH_3 on low-loaded MnO_x/Al_2O_3 catalysts [23]. Moreover, the formation of dinitrosyl and mononitrosyl species upon contacting NO with Mn_2O_3 were recently reported by Yamashita and Vannice [24]. In the Arrhenius plot of the NO reduction by propene a deviation of the activity level of $ZnMn_2O_4$ from the activity levels of the transition metal ions-doped catalysts occurs for temperatures higher than 773 K (see Fig. 5B). An XRD analysis was carried out on the catalyst after catalysis at temperatures equal or higher than 773 K. It revealed that the original spinel structure is preserved in the C_3H_8 containing stream but, by contrast, when propene is used as reductant of NO the original spinel structure is preserved only up to 773 K, because for temperature equal or higher than 773 K the spinel phase

collapses by reduction of Mn^{3+} to Mn^{2+} giving rise to a mixture of MnO and ZnO oxides. Also the spinels doped with copper and cobalt underwent reduction under the NO + C_3H_6 stream at a temperature equal or higher than 773 K but, by contrast, the iron doped catalyst appeared to be unreduced. With this respect it is fair to say that here some preliminary results of the catalytic properties of the iron doped catalysts and of its changes under reaction are given because this study is still in progress and it will be extensively reported in a next paper. Although the NO + C_3H_6 and H_2 reduction are reactions basically different in nature, it should be outlined how the stability under the catalytic reaction of the copper, cobalt and iron doped catalysts is well paralleled by their 'resistance' towards reduction in H_2 as found by TPR analysis. Surprisingly, in spite of the spinel reduction and the consequent disgregation into MnO and ZnO, the ZnMn-Cu(0.10) and ZnMn-Co(0.10) catalysts behave exactly as the starting monophasic spinels, this being clearly shown by the Arrhenius plots. Moreover, a careful inspection of the XRD patterns at the end of the catalytic run evidenced a systematic shift of both the MnO and ZnO diffraction peaks in opposite and, therefore, complementary direction. Thus, similarly to what found for the H_2 reduction, solid solutions of Zn^{2+} ions in MnO and Mn^{2+} ions in ZnO are formed upon collapsing of the spinel structure in the NO + C_3H_6 stream for temperature equal or higher than 773 K. We tried to explain these at first puzzling evidences by taking into account (i) the chemical properties of NO and C_3H_6 and (ii) the effect produced by their adsorption on the catalyst surface. If, on the one hand, the adsorption of propene can lead to a reduction of the surface, on the other hand the adsorption of NO, a rather strong oxidizing agent, is very likely to lead to an oxidation of the surface by forming N_2O and leaving an oxygen atom behind (vide infra). On this ground we speculate that, during the reaction with propene, NO may oxidize the Mn^{2+} ions in the disgregated catalysts, made by Zn^{2+}-MnO or Mn^{2+}-ZnO solid solutions, thus regenerating the Mn^{3+} active centre on the catalyst surface and preserving copper, or cobalt, in the still oxidized form. Indeed, no evidence of metal copper or cobalt were found in the disgregated catalysts. Our hypothesis is supported by the results reported by Shelef in a very elegant paper showing that the interaction of NO with the surface of MnO led to the oxidation, even at room temperature, of Mn^{2+} to Mn^{3+} with the simultaneous chemisorption of NO on the resulting Mn_2O_3 surface [25]. A similar oxidation mechanism by NO could be operative for the disgregated catalysts during the reaction with propene and may represent a possible explanation of the fact that the catalytic activity of the copper-, or cobalt-, doped spinel phases and the homologous disgregated catalysts is virtually the same. On the other hand, in the case of $ZnMn_2O_4$ the different behavior between the starting spinel and the disgregated sample is not immediate to explain. Although at this moment we could not turn out one of the following hypotheses, the surface density of the regenerated Mn^{3+} active sites, a change of their 'structure', or the absence of a redox equilibrium that might occur between manganese and copper, or cobalt, ions (vide infra) may be responsible of the changing in the catalytic activity.

3.3.2. Reduction of N_2O by propane or propene

The reduction of N_2O by propane or propene occurs efficiently over either undoped and doped catalysts. The selectivity to N_2 and CO_2 is always 100% in the whole range of temperature explored. The Arrhenius plots for the specific surface rate of N_2O reduction by C_3H_8 (Fig. 6A) and C_3H_6 (Fig. 6B) look rather different from those for the NO reduction. The activity lines are close to each other and, especially in the case of propane, the reaction appear to occur fairly the same way regardless the doping with the transition metal ion. When propene is used as reductant, however, a small split of the activity levels is observed. The copper doped catalyst shows a slight higher activity with both hydrocarbons whereas, if compared to the iron and cobalt catalysts, the undoped catalyst ($ZnMn_2O_4$) has a comparable or slightly higher activity when propane or propene are used as reductant, respectively. On the other hand, the slope of the activity levels either for the reactions with propane or propene does not differ too much

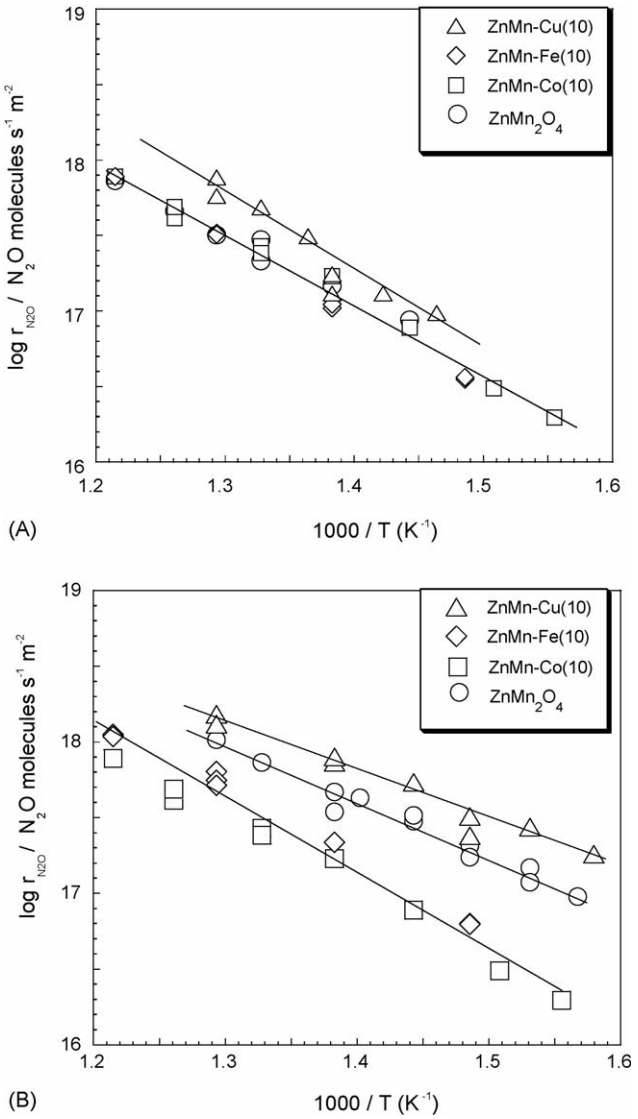

Fig. 6. Arrhenius plot of the N_2O reduction rates by C_3H_8 (A) and C_3H_6 (B) over the ZnMn-Me(0.10) catalysts. Reactant stream for the reduction [N_2O] = [C_3H_8] = [C_3H_6] = 4600 ppm + He balance (GHSV = 60,000 h^{-1}).

suggesting that the apparent activation energy is rather similar for all catalysts and is not influenced by doping the spinel with the transition metal ion. Furthermore, differently from what observed for the NO involving reactions, the activity levels of either the reduction of N_2O by both hydrocarbons or its decomposition (vide infra) are positioned at similar heights and have almost the same slope. These results, as a whole, suggest that the hydrocarbon, regardless if propane or propene are used, plays in the reaction only a marginal role and the N_2O decomposition step is the leading factor in the reaction mechanism (vide infra). As for NO, the catalysts are stable when propane is used as reductant but, also in this case with the only exception of the iron-zinc manganite, they collapse at temperature close or higher than 773 K under the propene containing stream by forming reciprocal MnO-ZnO solid solutions. Again, the disgregated catalysts, including $ZnMn_2O_4$, preserve the initial catalytic activity. This can be explained in perfect analogy with the hypotheses made for the $NO + C_3H_6$ reaction (vide supra).

3.3.3. NO and N_2O decomposition

The N_2O decomposition occurs over all catalysts in the whole range of temperature explored (523–873 K) while a significant activity for the NO decomposition appeared only at the highest temperature (see Fig. 7). With regard to N_2O reaction, the Arrhenius plots show that the catalytic activity of the undoped and doped catalysts is almost the same, only the ZnMn-Fe(0.10) catalyst being a slightly less active. On the other hand, for the NO decomposition the copper containing spinel is one order of magnitude more active than the iron, cobalt doped and undoped $ZnMn_2O_4$, all these latter being positioned at fairly the same point. If a comparison between the NO and N_2O decomposition reactions is made, it appears that

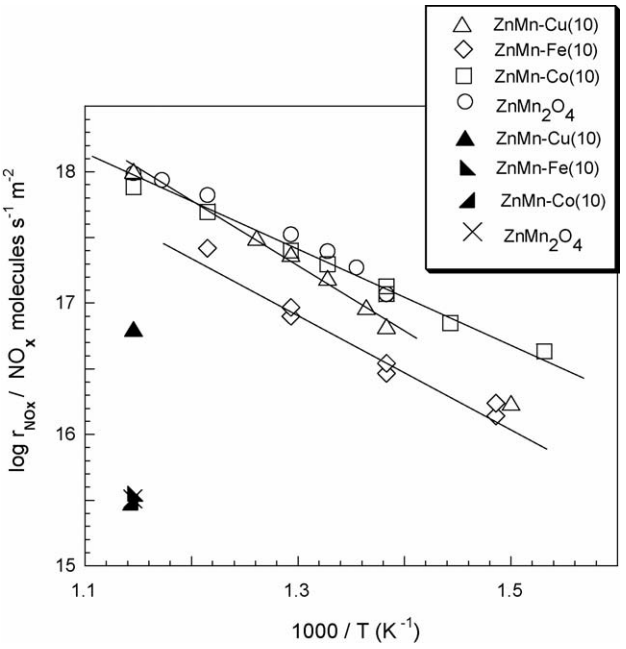

Fig. 7. Arrhenius plot of the N_2O decomposition rates (open symbols) and NO decomposition rates (closed symbols) over the ZnMn-Me(0.10) catalysts. Reactant stream $[N_2O] = [NO] = 4600$ ppm + He balance (GHSV = 60,000 h^{-1}).

the activity level for the NO decomposition is from one to two orders of magnitude lower than that of N_2O decomposition. Moreover, we found that the transformation of N_2O to N_2 occurs in the same way irrespective of the used hydrocarbon and, surprisingly, also in its absence in the reactant stream. It follows that the N_2O decomposition or reduction cannot be the rate determining step of the NO reduction or decomposition reactions. All these pieces of evidence, well matching the literature data [4,5,26,27], provide a picture that may be represented by the following reaction pathway:

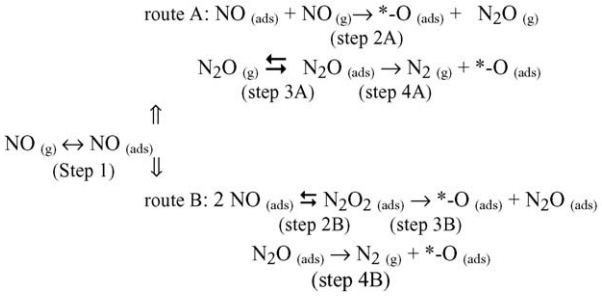

From the N_2O experiments we learned that, in the temperature range explored, steps 4A and 4B are 'facile' and occur easily both in presence or in absence of hydrocarbons. In other words the removal of the released adsorbed oxygen belonging to steps 4A and 4B is rather easy during the N_2O decomposition reaction, even with no help by reducing agents like propene or propane, suggesting that a mobile surface oxygen atom is involved in the reaction mechanism [27]. Our results are in agreement with previous one recently reported by Yamashita and Vannice [4] for the N_2O decomposition over manganese oxides. Indeed they found that, among the manganese oxides, Mn_2O_3 showed the highest activity, thus confirming that Mn^{3+} ions are the most effective manganese ions for this reaction as also well anticipated in the literature [28,29]. Therefore the good activity of undoped $ZnMn_2O_4$ found by us for the N_2O decomposition can be related to the presence of Mn^{3+} ions in the spinel structure. The same authors reported that also for the NO decomposition Mn_2O_3 was again the most active manganese oxide [5]. A comparison of our data with the results reported by Yamashita and Vannice [4,5] evidenced that at 623 K and at $P_{N_2O} = 0.0046$ atm the activity of $ZnMn_2O_4$ is more than 40 times higher than that of Mn_2O_3, and that the NO decomposition over $ZnMn_2O_4$ at 873 K and $P_{NO} = 0.0046$ atm is almost two orders of magnitude higher than that over Mn_2O_3, pointing to an influence of the solid structure on the catalytic activity. Yamashita and Vannice found also that the rate of NO decomposition is 700 times smaller than the rate of N_2O decomposition at 873 K and 0.04 atm of NO [5]. In agreement with these authors, we found a much lower reaction rate of NO decomposition with respect to N_2O decomposition over $ZnMn_2O_4$. All these results suggest that step 2A and/or 3B in our scheme is probably the rate determining step of the overall reaction. Finally, the catalytic results shows that the beneficial effect of the presence of transition metal ion is more evident for the catalysts doped with copper and in the case of

the reduction of NO by propane and propene. The internal redox equilibrium $Cu^{2+} + Mn^{3+} \leftrightarrow Cu^{1+} + Mn^{4+}$, existing in the $CuMn_2O_4$ spinel [30,31], could be operative also in the $Cu_xZn_{1-x}Mn_2O_4$ spinel and may play a role in enhancing its catalytic activity, for instance by favouring the charge transfer between the solid and the NO, or the hydrocarbon, adsorbed molecules. However similar redox equilibria might take place in the cobalt- and iron-doped zinc manganites, i.e. $Co^{3+} + Mn^{3+} \leftrightarrow Co^{2+} + Mn^{4+}$, or $Fe^{3+} + Mn^{3+} \leftrightarrow Fe^{2+} + Mn^{4+}$ thus affecting their catalytic behavior. On the other hand, the promoting effect of the hydrocarbons on the conversion of NO to N_2 is likely related to the fact that the removal of the adsorbed oxygen of step 2A and/or 3B is enhanced by a reducing agent. The released adsorbed oxygen of steps 4A and 4B does not need any reductant in order to be removed, as indeed shown by the N_2O experiments (see Fig. 6). This points to a different nature of the released adsorbed oxygen belonging to steps 2A and 3B as compared to those belonging to steps 4A and 4B, in other words at the surface the bonding strength of the formers is much higher than that of the latters.

4. Conclusions

4.1. Precursor and catalyst characterization

By coprecipitation at constant pH of suitable amounts of zinc and manganese, all alone or plus iron, or cobalt or copper, monophasic carbonate precursors are obtained having the $MnCO_3$ (rhodochrosite)-type structure in which Zn^{2+}, or Co^{2+} or Cu^{2+}entered in solid solution. Surprisingly, iron is mostly present in the rhodochrosite crystal lattice as Fe^{3+} ions and only a small amount of Fe^{2+} was found. Upon thermal decomposition of the carbonate precursors in air at 723 and 973 K, all the Mn^{2+} ions were oxidized to Mn^{3+} ions and a zinc manganite phase, $ZnMn_2O_4$, characterized by a tetragonal spinel-like structure, is obtained at both temperatures. Regardless the presence of the transition metal ion, its nature and content, all the calcined samples are still monophasic being made only by the spinel phase. Upon calcination, in the transition metal ion doped catalysts all iron and cobalt turn completely into Fe^{3+} and Co^{3+} ions that are located in the octahedral sites of the spinel structure together with Mn^{+3} ions. On the other hand, in the copper doped catalyst the Cu^{2+} ions occupy the tetrahedral sites together with the Zn^{+2} ions.

4.2. H_2 reduction behavior

The catalyst reduction in H_2 is affected by the doping with the transition metal ions that, depending on their nature, played a different role. For the set of samples prepared at 723 K, compared to pure zinc manganite, the effect on the spinel reduction of the hosted transition metal ion brings out the following remarks: (i) the reduction is inhibited by iron in some extent, (ii) it was almost unchanged by cobalt and (iii) it is markedly enhanced by copper. On the other hand, the solids obtained at 973 K are more hardly reduced than the homologous samples calcined at 723 K owing to the larger particle size obtained on increasing the calcinations temperature. Regardless the calcination temperature and the doping with transition metal ions, the reduction occurred in a single step with the only exception of the ZnMn-Cu(0.10) catalyst calcined at 973 K. In consequence of the reduction the initial spinel phase disgregated forming ZnO and MnO as reciprocal solid solutions.

4.3. Catalytic behavior

Zinc manganite, pure or doped with iron, or cobalt or copper, is an active catalysts for the NO reduction by propane and propene. For all catalysts at 873 K the selectivities to N_2 and CO_2 are equal to 1. At temperatures lower than 873 K propene is more efficient than propane in reducing NO but the selectivity to N_2 decreases being N_2O also formed. The presence of the transition metal ions enhances the catalytic activity and the following scale of decreasing activity can be drawn:

$$\text{ZnMn-(Cu)} > \text{ZnMn-(Fe)} > \text{ZnMn-(Co)} > \text{ZnMn-Me(0)}$$

The catalytic data clearly indicate that Mn^{3+} ions are the active species as well as Cu^{2+}, or Fe^{3+}, or Co^{3+} ions. The catalytic activity for the NO decomposition, if compared to the NO reduction by hydrocarbons, was significantly lower. The reduction of N_2O by propane or propene occurs efficiently over either undoped and doped catalysts with selectivities to N_2 and CO_2 equal to unity in the whole range of temperature explored. Compared to NO, the N_2O reduction by hydrocarbons is much less affected by the doping of the catalysts, especially in the case of propane. On the other hand, the N_2O reduction by propane, or propene, and its decomposition are characterized by a similar activity, suggesting that the oxygen atom released at the catalyst surface by N_2O is easily removed even in absence of a reductant. The results found for the NO and N_2O reactions suggest, as a whole, that two different types of adsorbed oxygen are involved in the reaction mechanism of NO reduction by hydrocarbons: one more firmly retained at the catalyst surface and the other one characterized by a high mobility. All catalysts are stable in the whole range of temperature explored when propane is contained in the reactant stream. By contrast when propene was used as reductant the original catalyst structure was preserved up to about 773 K but, with the only exception of iron-doped catalyst, for temperatures equal or higher than this value the monophasic catalysts disgregated by reduction forming a complex mixture of MnO and ZnO oxides and their reciprocal solid solutions. In spite of collapsing of the initial monophasic spinel phase, the polyphasic catalysts still maintained a good catalytic activity. This surprising continuity was explained by suggesting that the Mn^{3+} active species might be regenerated in the reactant stream through the surface oxidation of Mn^{2+} ions in MnO or in solid solution in ZnO.

References

[1] V.I. Pârvulescu, P. Grange, B. Delmon, Catal. Today 46 (1998) 233.
[2] F. Kapteijn, J. Rodriguez-Mirasol, J.A. Moulijn, Appl. Catal. B Environ. 9 (1996) 25.

[3] F. Kapteijn, L. Singoredio, A. Andreini, J.A. Moulijn, Appl. Catal. B Environ. 3 (1994) 173.
[4] T. Yamashita, A. Vannice, J. Catal. 161 (1996) 254.
[5] T. Yamashita, A. Vannice, J. Catal. 163 (1996) 158.
[6] W. Sjoerd Kijlstra, D.S. Brands, E.K. Poels, A. Bliek, J. Catal. 171 (1997) 208.
[7] W. Sjoerd Kijlstra, D.S. Brands, H.I. Smit, E.K. Poels, A. Bliek, J. Catal. 171 (1997) 219.
[8] W. Sjoerd Kijlstra, M. Biervliet, E.K. Poels, A. Bliek, Appl. Catal. B Environ. 16 (1998) 327.
[9] G. Fierro, S. Morpurgo, M. Lo Jacono, M. Inversi, I. Pettiti, Appl. Catal. A General 166 (1998) 407.
[10] G. Fierro, M. Lo Jacono, M. Inversi, R. Dragone, G. Ferraris, Appl. Catal. B Environ. 30 (2001) 173.
[11] G. Fierro, M. Lo Jacono, R. Dragone, G. Ferraris, G.B. Andreozzi, G. Graziani, Solid State Phenom. 90-91 (2003) 153.
[12] G. Fierro, M. Lo Jacono, M. Inversi, P. Porta, R. Lavecchia, F. Cioci, J. Catal. 148 (1994) 709.
[13] D.A.M. Monti, A. Baiker, J. Catal. 83 (1983) 323.
[14] P. Malet, B. Caballero, J. Chem. Soc. Faraday Trans. 1 (84) (1988) 2369.
[15] G. Ferraris, G. Fierro, M. Lo Jacono, M. Inversi, R. Dragone, Appl. Catal. B Environ. 36 (2002) 251.
[16] R.D. Shannon, Acta Crystallogr. Sect. A 32 (1976) 751.
[17] I.S. Iacobs, J.S. Kouvel, Phys. Rev. 122 (1961) 412.
[18] B. Boucher, R. Buhl, M. Perrin, J. Phys. Chem. Solids 32 (1971) 2429.
[19] G. Fierro, M. Lo Jacono, M. Inversi, R. Dragone, P. Porta, Topics Catal. 10 (2000) 39.
[20] G.L. Castiglioni, A. Vaccari, G. Fierro, M. Inversi, M. Lo Jacono, G. Minelli, I. Pettiti, P. Porta, M. Gazzano, Appl. Catal. A General 123 (1995) 123.
[21] G. Fierro, M. Lo Jacono, M. Inversi, G. Moretti, P. Porta, R. Lavecchia, in: L. Guczi, F. Solymosi, P. Tétényi (Eds.), Proceedings of the 10th International Congress on Catalysis, joint edition by Elsevier Science Publishers, Amsterdam, The Netherlands, and Akadémiai Kiadó, Budapest, Hungary, 1993, Part B, p. 283.
[22] G. Fierro, M. Lo Jacono, M. Inversi, P. Porta, F. Cioci, R. Lavecchia, App. Catal. A General 137 (1996) 327.
[23] W.S. Kijlstra, E.K. Poels, A. Bliek, B.M. Weckhuysen, R.A. Schoonheydt, J. Phys. Chem. B 101 (1997) 309.
[24] T. Yamashita, M.A. Vannice, Appl. Catal. B Environ. 13 (1997) 141.
[25] H.C. Yao, M. Shelef, J. Catal. 31 (1973) 377.
[26] A. Amirnazmi, J.E. Benson, M. Boudart, J. Catal. 30 (1973) 55.
[27] K.J. Lim, D.G. Loffler, M. Boudart, J. Catal. 100 (1986) 158.
[28] A. Cimino, F.S. Stone, in: G. Ertl, H. Knozinger, J. Weitkamp (Eds.), Handbook of Heterogeneous Catalysis, 2, VCH Publishers, Weinheim, 1997, p. 848.
[29] A. Cimino, F.S. Stone, Adv. Catal. 47 (2002) 141.
[30] S. Veprek, D.L. Cocke, S. Kehl, H.R. Oswald, J. Catal. 100 (1986) 250.
[31] P. Porta, G. Moretti, M. Musicanti, A. Nardella, Solid State Ionics 63–65 (1993) 257.